applied mechanics

MDPI

Article

An Integrated Approach for Designing and Analyzing Lumbar Vertebral Biomodels with Artificial Disc Replacement

Mhd Ayham Darwich [1,2], Katreen Ebrahem [1,2], Maysaa Shash [1,2], Hasan Mhd Nazha [3,*], Szabolcs Szávai [4], Yicha Zhang [5] and Daniel Juhre [3]

[1] Faculty of Biomedical Engineering, Al-Andalus University for Medical Sciences, Tartous P.O. Box 101, Syria; a.darwich@au.edu.sy (M.A.D.); ci41@au.edu.sy (K.E.); ms11@au.edu.sy (M.S.)
[2] Faculty of Technical Engineering, University of Tartous, Tartous P.O. Box 2147, Syria
[3] Institute of Mechanics, Faculty of Mechanical Engineering, Otto Von Guericke University Magdeburg, Universitätsplatz 2, 39106 Magdeburg, Germany; daniel.juhre@ovgu.de
[4] Institute of Machine and Product Design, Faculty of Mechanical Engineering and Informatics, University of Miskolc, 3515 Miskolc, Hungary; szavai.szabolcs@uni-miskolc.hu
[5] Mechanical Engineering and Design Department, Université de Technologie de Belfort-Montbéliard, ICB UMR CNRS 6303, 90010 Belfort, France; yicha.zhang@utbm.fr
* Correspondence: hasan.nazha@ovgu.de

Abstract: This study aims to develop an integrated approach for 3D lumbar vertebral biomodel design and analysis, specifically targeting unilevel disc degeneration and the replacement of lumbar artificial discs. Key objectives include improving existing design methods through 3D techniques, inverse modeling, and an engineering biomodel preparation protocol. Additionally, the study evaluates mechanical properties in the implantation area and between disc components to gauge the effectiveness of artificial discs in restoring functional movement within the studied biological model. The construction of a biological model representing the L3–L4 functional spinal unit was based on measurements from radiographic images and computed tomography data obtained from the study sample. The 3D finite element method in Ansys software (v. 19.2, ANSYS, Inc., Canonsburg, PA, USA) was used to monitor the distribution of equivalent stress values within the core of the two artificial discs and the behavior of vertebral bone components in the model. This approach enabled the creation of personalized digital models tailored to the specific implantation requirements of each patient. Stress analysis identified critical areas within the disc cores, suggesting potential design modifications to optimize artificial disc performance, such as selectively increasing core thickness in specific regions and considering adjustments during implantation. For example, preserving part of the lateral annulus fibrosus from the degenerative disc and maintaining the anterior and posterior longitudinal ligaments may play a crucial role in balancing the forces and moments experienced by the lumbar section. This study provides valuable insights into the development of patient-specific solutions for lumbar disc degeneration cases, with the potential for enhancing artificial disc design and implantation techniques for improved functional outcomes.

Keywords: artificial lumbar disc; lumbar total disc replacement (LTDR); finite elements analysis (FEA)

Citation: Darwich, M.A.; Ebrahem, K.; Shash, M.; Nazha, H.M.; Szávai, S.; Zhang, Y.; Juhre, D. An Integrated Approach for Designing and Analyzing Lumbar Vertebral Biomodels with Artificial Disc Replacement. *Appl. Mech.* **2023**, *4*, 1227–1239. https://doi.org/10.3390/applmech4040063

Received: 29 October 2023
Revised: 20 November 2023
Accepted: 6 December 2023
Published: 8 December 2023

1. Introduction

Degenerative disc disease is a prevalent source of chronic low back pain, often necessitating therapeutic intervention. A pivotal development in addressing this condition traces back to 1960 when total disc replacement (TDR) systems were introduced, revolutionizing treatment options with artificial instruments. TDR involves the replacement of a damaged disc with an artificial disc (AID), aiming to restore disc height, correct segmental inclination, and maintain range of motion. Recent studies have underscored the escalating significance of TDR [1,2]. These studies encompass a spectrum of research methodologies, including

experimental investigations and finite element analyses, the latter gaining prominence due to its cost-effectiveness in deciphering the biomechanics of biological models.

The implantation of artificial discs presents a critical challenge to prosthetic experts. The slightest positional error can lead to mechanical mismatches with spine movement, particularly during lateral bending and axial rotation. Furthermore, cyclic loading conditions can trigger bone osteolytic and inflammatory responses because of wear debris generation [3].

TDR systems comprise bearing surfaces engineered to withstand loading without fracturing, minimize friction and wear, and preserve an extended range of motion [4]. These TDR models can be systematically categorized based on design, fixation, friction pairs, the location of the center of motion, and compatibility with MRI. Regarding design, the regular disc exhibits six degrees of freedom, divided into three in displacement and three in rotation. Consequently, we identified three distinct design types: Firstly, free design (6 degrees of freedom). These are exemplified by the LP-ESP® product, which represents the lumbar disk prosthesis-elastic spine pad (Spine Innovations, Mulhouse, France), and do not necessitate perfect centering but exert greater pressure on the posterior joints. Secondly, semi-constrained design (5 degrees of freedom) with a free core, such as Charité® (DePuy Synthes, Raynham, MA, USA) and Mobidisc® (Zimmer Biomet, Warsaw, IN, USA); these are stable designs where displacement occurs within the core and increases with the core's radius. Thirdly, constrained design (3 degrees of freedom) with a fixed core. As exemplified by the Maverick® ProDisc-L® (Medtronic Ltd., Dublin, Ireland) these require exceptional stability and hence perfect fixation [5].

Fixation is crucial for all prostheses, necessitating both short and long-term solutions. At a macro level, fixation can be achieved through immediate fusion using stems, keels, screws, macrostructures, or porous surfaces, with surface coatings facilitating osseointegration. Materials like hydroxyapatite, tricalcium phosphate, porous titanium, and chromium-cobalt can enhance fixation. On a microscopic scale, long-term biological incorporation is indispensable to ensure the lifetime stability of the prosthesis, with certain materials exhibiting superior performance in this regard, particularly for prostheses with constrained designs that transmit greater forces to the vertebral endplates [6].

The choice of friction pair is pivotal, with four options available: metal/PE (Polyethylene), ceramic/PE, metal/metal, and ceramic/ceramic. Notably, the metal/PE bearing, which is the oldest bearing used in industrial prostheses, yields larger particles from PE debris, while the metal/metal and ceramic/ceramic bearing debris generates fewer and smaller particles [7]. Moreover, certain TDR models have a center of rotation located either below or above the disc being replaced, with ceramic/PE and ceramic/ceramic models being most compatible with magnetic resonance imaging (MRI) [8].

To determine the material properties of any prosthesis, it is imperative to ascertain the anticipated requirements. In the context of total disc arthroplasty, these requirements center around preserving or re-establishing functional disc motion while minimizing implant wear and failure. Given that the intervertebral disc and surface joints collectively form a three-joint system, it is crucial to ensure that the artificial disc replacement adequately complements their functions. Additionally, considerations must be made for site-specific mobility and load requirements, considering the disparities between lumbar and cervical disc replacements in terms of load capacity, natural motion patterns, and ranges of motion [9].

Bearing materials must not only facilitate movement but also distribute loads with low friction and high wear resistance. The risk of osteolysis, akin to that observed in hip and knee replacements, is directly related to factors such as particle size, particle density, surface chemistry, and the types of tissues in contact with the prosthesis. It is imperative to explore specific bearing surfaces such as articulated joints (Metal-on-Plastic, MOP) and newer bearings like MOM (Metal-on Metal) to mitigate osteoporosis's severity [10].

The choice of implant material can significantly impact postoperative imaging. Titanium and its alloys are generally superior to stainless steel and cobalt-chromium alloys,

as they result in fewer artifacts during imaging. Given the continuous movement around disc prostheses and the potential for subsequent degenerative and osseous changes, the ability to conduct postoperative imaging is of growing concern as the use of such implants expands [11].

The current landscape of materials used in total disc replacement predominantly includes cobalt-chromium alloys, titanium alloys, stainless steel, polyethylene, polyurethane, and ceramics. Notably, ultra-high molecular weight polyethylene (UHMWPE) is the most used polymeric material for orthopedic bearing surfaces [12].

Traditional treatments for degenerative disc diseases can be physically and financially taxing, with long-term results. Surgical options, such as spinal fusion surgery, are widely accepted as efficacious interventions. However, they may come with high costs, mobility limitations, decreased disc height, and the potential for damage in the adjacent plane [13]. These factors can contribute to changes in the biomechanical environment and spinal instability.

Clinical evaluations of artificial discs in a biological environment encompass physical examinations, visual analog scale assessments for back pain (VAS), and the Oswestry index (ODI). Radiological evaluations involve X-rays, CT (Computed Tomography) scans, and MRI scans [14]. These radiographic parameters encompass intervertebral disc height (IDH), range of motion (ROM), lumbar lordosis, and substitution site [15]. To gain insights into the mechanical response, stress distribution, and deformations of lumbar prostheses under static loads, numerical analysis methods based on finite elements are employed [16]. These analyses also encompass the evaluation of loading states during natural spinal movements, such as axial rotation, flexion/extension, lateral bending, and axial loading [17]. Additionally, finite element analysis is leveraged to study the optimal design of the core of lumbar intervertebral discs [5,13,14] and to explore the biomechanical effects of the geometry of the ball-on-socket artificial disc in the lumbar section [10,16].

Numerical finite-element analysis methods have further been utilized in validation studies to assess the preoperative modeling of total disc replacement surgery [18]. They have been instrumental in predicting prosthetic wear for various materials [19] and have enabled comparative in vivo analyses of the prosthesis within the biological environment [20].

The current study is positioned within the realm of three-dimensional computer evaluation, offering an integrated methodology for assessing artificial discs dedicated to the lumbar region. This methodology leverages mechanical design data obtained through computerized tomography (CT) and three-dimensional mechanical design programs. Employing the 3D finite element method, the study aims to scrutinize the resulting model, considering the impact of disc manufacturing materials and the behavior of bone material. Ultimately, the study seeks to refine the process of disc implantation by methodically applying the replacement and comprehensively understanding the biomechanics of replacement discs within the biological environment. Such an approach aligns with scientific standards and precise techniques, with the goal of enhancing the clinical outcomes and investment in this field.

2. Materials and Methods

2.1. Study Sample

The study sample comprises individuals suffering from chronic low back pain, with varying degrees of unilevel disc degeneration. For this research, a representative model was chosen—a 38-year-old male with disc degeneration at the (L3–L4) spinal level. The selected sample exhibited normal vertebral bodies, the absence of advanced spinal diseases (e.g., slipped vertebrae or disc collapse), and no history of prior spinal surgeries. Utilizing a series of CT scans converted to a DICOM (Digital Imaging and Communications in Medicine) file format, the (L3–L4) model was generated in Materialize MIMICS software. Subsequently, the model was imported into SolidWorks CAD (Version 2019; Dassault Systèmes SolidWorks Corporation, Vélizy-Villacoublay, France) in STEP file format, forming the basis for the finalized element model used in this study.

2.2. Model Generation

The intervertebral disc prostheses were meticulously designed to fit within the (L3–L4) intervertebral space. The 3D models of both discs were crafted using SolidWorks (Version 2019; Dassault Systèmes SolidWorks Corporation, France), adhering to the dimensions of the anteroposterior diameter (AP) and the mediolateral diameter (ML) of the endplates of the study model. Specifically, ball-on-socket designs approved by the Food and Drug Administration were selected with precise measurements, as depicted in Figure 1.

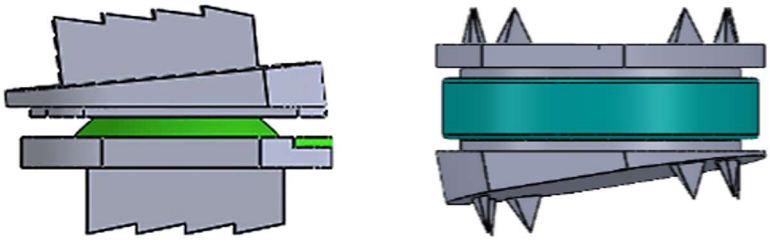

Figure 1. Precision-crafted intervertebral disc prostheses designed for (L3–L4) interbody fusion.

2.3. Validation Study

Various regions were assigned to the vertebrae, including the upper and lower endplates, cancellous bone, cortical bone, and posterior bone (Figure 2).

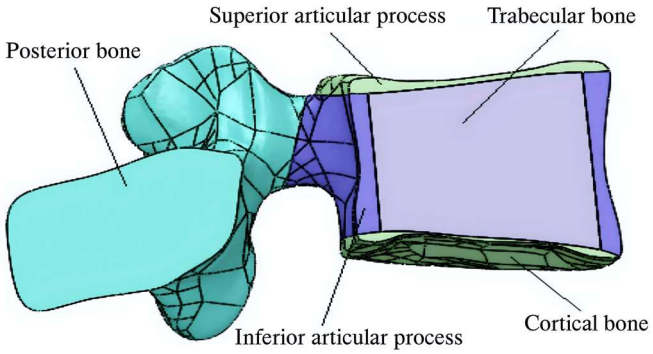

Figure 2. Regional assignments for vertebrae, including endplates, trabecular bone, cortical bone, and posterior bone.

Additionally, seven essential ligaments connecting the vertebral bodies were incorporated into the model. These ligaments included the anterior longitudinal ligament (ALL), posterior longitudinal ligament (PLL), ligament (LF), capsular ligament (CL), supraspinal ligament (SS), interspinous ligament (IS), and transverse ligament (TL). Grooves were created on the surfaces of the lower endplate of the vertebra (L3) and the upper endplate of the vertebra (L4) along the mid-sagittal line to facilitate disc replacement. The ProDisc-L disc was inserted in a posterior position with a (4 mm) gap, while the CHARITÉ disc was positioned anteriorly [21].

The simulation included the removal of both anterior and posterior longitudinal ligaments, replicating the procedure used during disc implantation. A critical aspect in the finite element modeling process involved ensuring that the mesh elements' density and shape were appropriately optimized to attain solution convergence. Insufficient mesh refinement can lead to inaccuracies, particularly when reducing the volume mesh, and may result in the presence of small analysis elements along the edges and within narrow anatomical features [22]. The upper and lower endplates of the ProDisc-L and CHARITÉ discs were represented as rigid bodies in the model [23]. In our study, hexahedral elements were utilized for constructing the mesh, while quadrilateral elements were employed for the

core mesh [22]. The mesh sizes were systematically reduced, leading to finer discretization. The convergence was monitored by assessing the changes in the results as the mesh was refined. The convergence criteria were set such that the variation in the results reached less than 1% with respect of the change in mesh size. This was achieved by carefully refining the mesh until a consistent solution was obtained. Table 1 provides a detailed number of the nodes and elements after refinement for the various components of the vertebrae and disc models for both ProDisc and CHARITÉ implant cases. The resultant representative model of the implant bio-environment was then exported to Ansys software (v. 19.2, ANSYS, Inc., Canonsburg, PA, USA) to conduct finite element analysis (FEA), as shown in Figure 3.

Table 1. Detailed element counts in vertebrae and disc models for ProDisc and CHARITÉ implant cases, including ligaments and groove configurations.

Component		Elements	Nodes	Component		Elements	Nodes
L3	Cortical bone	3135	6148	L3	Cortical bone	3299	6465
	Cancellous bone	528	1062		Cancellous bone	372	787
	Lower endplate1	991	2100		Lower endplate	2287	4582
	Lower endplate2	1218	2469		Upper endplate	1215	2563
	Upper endplate	1139	2391		Posterior bone	6643	12,227
	Posterior bone	4885	9059		Cortical bone	2259	4560
L4	Cortical bone	2502	4947	L4	Cancellous bone	503	1022
	Cancellous bone	556	1103		Lower endplate	1321	2801
	Lower endplate	915	1966		Upper endplate	635	1438
	Upper endplate1	459	1054		Posterior bone	5720	10,467
	Upper endplate2	412	968		Core	29,517	48,609
	Posterior bone	3584	6662		Lower endplate	373	1163
ProDisc-L	Core	2555	1521	CHARITÉ	Upper endplate	378	1196
	Lower endplate	148	369		Cortical bone	3299	6465
	Upper endplate	307	734		Cancellous bone	372	787

(**A**) (**B**)

Figure 3. Bio-environment modeling with ligaments and disc placement for finite element analysis (FEA). (**A**) ProDisc model; (**B**) CHARITÉ model.

2.4. Boundary Conditions

A compressive load of 500 N was applied to the upper endplate of a vertebra (L3) to simulate physiological compressive loading. The lower endplate of a vertebra (L4) was fully fixed. To mimic the goal of total disc replacement (TDR) in restoring range of motion, a moment of 7.5 N. m was applied at three anatomical levels to simulate flexion, extension, lateral bending, and axial rotation movements. For the ProDisc-L disc, the core's base is connected to the lower endplate of the disc. The contact state is established between the upper endplate of the disc and the core for ProDisc-L, and between the surfaces of both the upper and lower endplate disc and the core for the CHARITÉ replacement. A

Coulombic friction coefficient ($\mu = 0.083$) typical for surface bearings (CoCr-UHMWPE) is applied [24]. Additionally, complete bonding is set for the interface surfaces, simulating bone growth within the implant area to represent complete fusion. A sliding connection contact is established in the facet joints between the two vertebrae [22].

2.5. Materials Properties

The outcomes of the experiments rely on the physical, mechanical, and thermal characteristics of the materials employed. It was assumed that both the bone structures and the alternative discs used for the components under investigation exhibit isotropic linear elasticity and homogeneity [25,26]. In Tables 2 and 3, the material properties of the components included in this research are presented, derived from reference values from previous studies [21,22,27,28].

Table 2. Material properties of investigated components based on assumed isotropic linear elasticity and homogeneity.

Material	Density (g/cm^3)	Young Modulus (MPa)	Poisson Ratio
Cortical bone	1.7	12,000	0.3
Cancellous bone	1.1	100	0.2
Posterior bone	1.4	3500	0.25
Upper and lower endplate	1.7	12,000	0.3
CoCrMo alloy	8.9	210,000	0.3
UHMWPE	0.94	1200	0.46

Table 3. Material properties of investigated ligaments.

Material	Density (g/cm^3)	Young Modulus (MPa)	Poisson Ratio	Cross-Section Area (mm^2)
LF	1	50	0.3	60
TL	1	50	0.3	10
IS	1	28	0.3	35.5
SS	1	28	0.3	35.5
CL	1	20	0.3	40

3. Results

3.1. Range of Motion

The range of motion (ROM) was meticulously examined in this study, representing the total angular rotation of vertebra L3. We assessed the ROM in various movements, including flexion/extension, lateral bending, and axial rotation. The findings, as illustrated in Figure 4, are particularly noteworthy.

The analysis demonstrated a significant agreement between the FEM results and those derived from a prior reference study examining conditions of normal lumbar movement [29], which will be further elucidated in the subsequent discussion section. This agreement underscores the efficacy of the ball-and-socket design of the two alternative discs, ProDisc-L and CHARITÉ, in restoring motion. Notable observations for each prosthetic disc include:

ProDisc-L: This model exhibited a substantial increase in range of motion (1.8°) during axial rotation, exceeding the normal range by 1.5 times. The absence of initial movement segment constraints during axial rotation, such as keeping part of the annulus fibrosus of the damaged disc or anterior longitudinal ligaments, likely contributes to this increase [30]. Furthermore, the ProDisc-L prosthesis demonstrated an enhanced range of motion (2.7°) in extension compared to the normal range (1.125 times), possibly due to the complete removal of the disc along with the anterior and posterior longitudinal ligaments. These ligaments

are vital structures for countering extension moments, rendering extension movement in the implant plane more flexible [31].

In contrast, the CHARITÉ model replicated the physiological behavior of the natural disc, particularly concerning the instantaneous center of rotation [32].

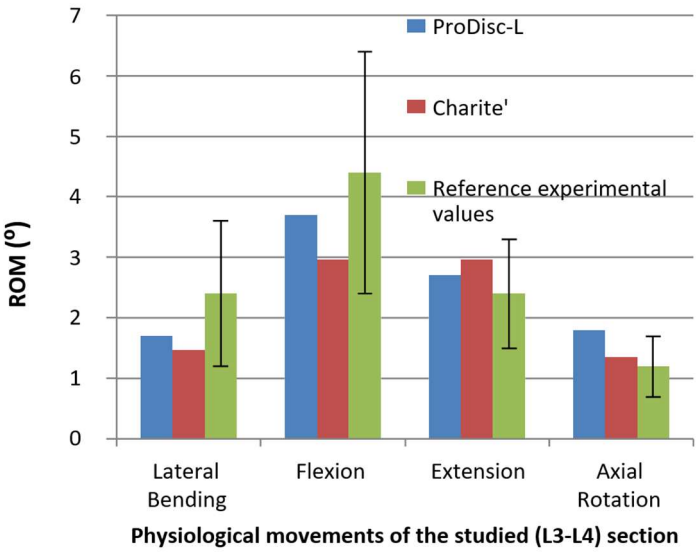

Figure 4. A chart of comparison of angular range of motion between the finite element method (FEM) results and experimental data, accompanied by standard deviation values.

3.2. Stress Distribution

The mechanical properties of the bearing materials for both disc types significantly influenced the expected lifespan of the replacement. The core material's structural integrity under mechanical loads was thoroughly investigated. Figures 5 and 6 depict the stress distribution within the core material.

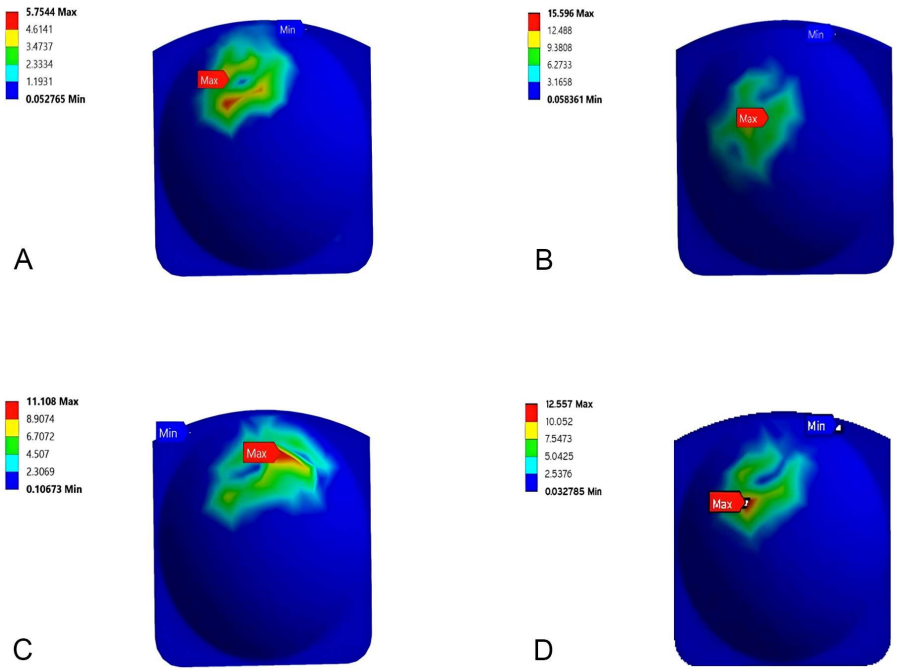

Figure 5. This image illustrates the distribution of von Mises stresses on the bearing surface of a UHMWPE core in the ProDisc-L model during various movements, including (**A**) flexion, (**B**) extension, (**C**) lateral bending, and (**D**) axial rotation.

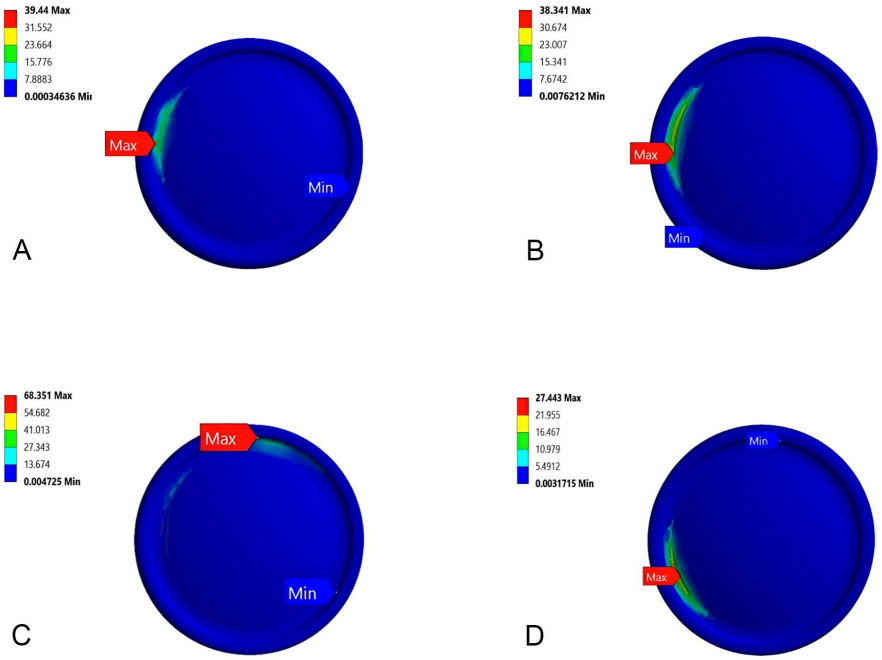

Figure 6. The distribution of von Mises stresses on the bearing surface of a UHMWPE core in the CHARITÉ model under the same movements, including (**A**) flexion, (**B**) extension, (**C**) lateral bending, and (**D**) axial rotation.

In the case of the ProDisc-L, forward loads were evenly distributed during flexion, owing to the large contact area. Extension movements, however, caused changes in the contact area, leading to differing stress patterns. Conversely, the CHARITÉ disc exhibited maximum stress values around the circumferential edge of the core during all movements, particularly at the area of local minimum thickness, as shown in Figure 7. This area has been identified as a vulnerable site, potentially prone to plastic deformation, wear, and fracture [33].

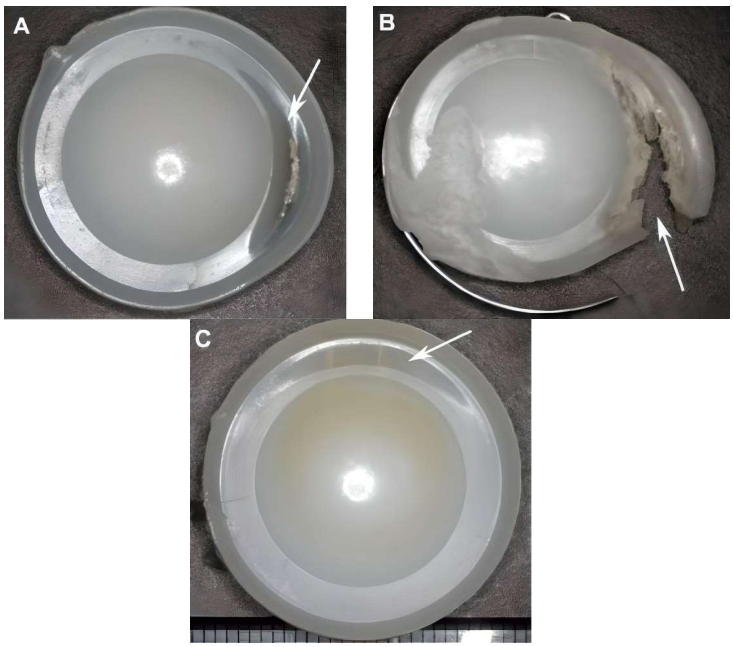

Figure 7. Damage to the edges of the core of the total disc replacement in retrieval studies [31] with permission from Elsevier (License Number: 5658170448214): (**A**,**C**) Polishing, plastic deformation, and transverse crack. (**B**) Transverse crack and edge fracture.

Figure 8 illustrates the maximum von Mises stress values for both ProDisc-L and CHARITÉ during various physiological movements. Notably, the maximum von Mises stress on the CHARITÉ disc reached 68 MPa at a depth of 0.01 mm during axial rotation. This level of stress may pose a risk to the disc under the applied loading conditions, as previous research has reported a yield stress value for high molecular weight polyethylene of 21 MPa [34].

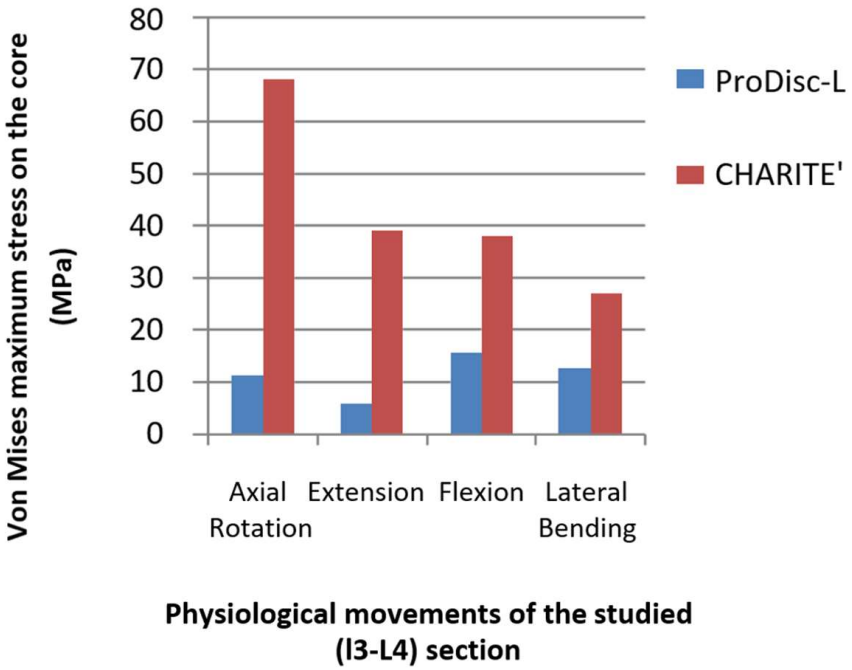

Figure 8. Diagram of the maximum (von Mises) stress values on the surface of the bearing core (UHMWPE) for both ProDisc-L and CHARITÉ during the physiological movements of the studied section.

In contrast, all FEM results for the ProDisc-L core remained below this yield stress value, with a maximum stress value of 15.6 MPa during flexion, ensuring that the core will not deform. To prevent stress concentration and potential damage in the CHARITÉ disc core, reinforcing specific areas or increasing thickness is advisable.

3.3. Bone Fracture Analysis

The study delved into the ability of bone to withstand fractures under the influence of applied kinematics during movement. This resilience is determined by the mechanical properties of bone, its composite structure, and organization.

When analyzing the stress–strain behavior of bone material, it became apparent that the performance of bone varies in both elastic and plastic regions [35]. Elastic regions exhibit stress storage and flexibility at lower-level strains, while the plastic region leads to bone material deformation and the possibility of damage, such as the formation of microcracks (Figure 9).

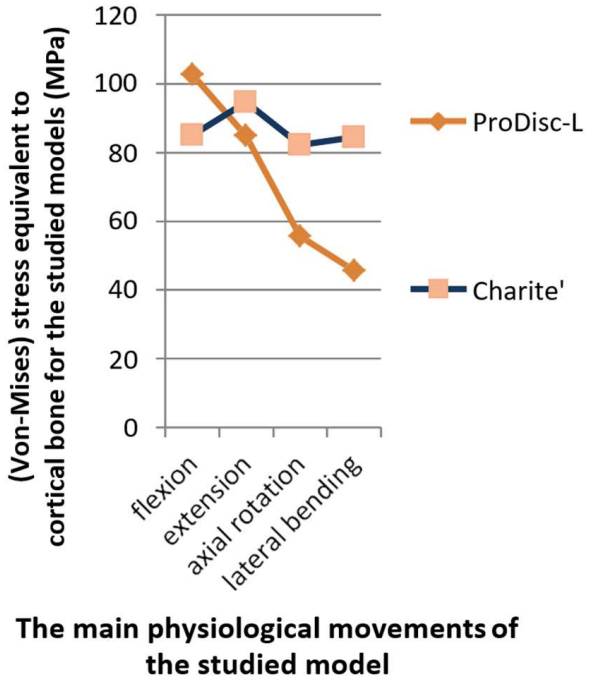

Figure 9. A chart displaying the equivalent von Mises stress values for both models during physiological movements.

Cortical bone, stronger but less flexible, can endure higher stresses and lower strains before failure. On the other hand, the porous nature of cancellous bone seems to provide greater flexibility but bears lower stress levels with significantly higher strains before failure [36]. The von Mises yield criterion, based on the distortion energy theory, was employed to investigate the stresses occurring on the cortical side of the bone, which behaves as a ductile material [37].

The yield stress values for bone material when tested by compression were found to exceed the minimum stress required for bone in general and cortical bone. Consequently, the bone material in both vertebrae of the studied models exhibited no plastic deformation in all motion tests [38].

4. Discussion

The evaluation of range of motion (ROM) in this study has provided valuable insights into the performance of ProDisc-L and CHARITÉ prosthetic discs, with a specific emphasis on the validation aspect assessed through several comparisons with the relevant clinical and experimental studies. The analysis not only demonstrated a substantial agreement between the finite element method (FEM) results and those from a preceding reference study on normal lumbar movement conditions but also contributed to the validation of our findings compared to previous experimental and clinical investigations.

In general, both prosthetic discs exhibited the ability to maintain range of motion across all three main levels, showcasing the motion-restoring capacity inherent in the ball-on-socket design employed in the ProDisc-L and CHARITÉ discs. This observation aligns with findings from a study on the Dynesys system, which highlighted the system's impact on intervertebral rotations, intersegmental ROM, neutral zone (NZ), and three-dimensional helical axis of motion (HAM) [29]. In concordance with the findings of the Dynesys system which caused a reduction in ROM values and restoration of NZ values, the ProDisc-L discs seemed to demonstrate a 1.8° increase in the range of motion, indicating a 1.5-fold improvement, notably in the axial rotation. This increase may be attributed to the absence of initial segment constraints during axial rotation, as supported by previous studies [30].

However, the ProDisc-L also exhibited an increase in range of motion (2.7°) in extension, which was 1.125 times greater than the normal range. This outcome may be attributed

to the complete removal of the entire disc along with the anterior and posterior longitudinal ligaments, structures essential for countering extension moments. The absence of these structures rendered the extension movement in the implant plane more flexible. Additionally, the ProDisc-L displayed a reduced range of motion in flexion compared to the natural disc, possibly due to differences in the momentary axis of rotation during movement in the sagittal plane.

In contrast, the CHARITÉ model replicated the physiological behavior of the natural disc, particularly concerning the instantaneous center of rotation [32]. The study emphasized the critical role of bearing materials for the expected life of disc replacements, with the CHARITÉ disc experiencing the highest stress values at the circumferential edge of the disc core during various movements. This vulnerable area, identified in a previous study [33], raises concerns about potential issues such as plastic deformation, wear, and fractures.

The study also conducted bone fracture analysis, exploring the mechanical properties of bone material under varying loads. Both the ProDisc-L and CHARITÉ discs generated stress values below the yield point of bone material, ensuring that bone material in the studied models did not deform plastically during the various motion tests. Importantly, the stress values were well below the minimum stress field that bone, especially cortical bone, can tolerate, emphasizing the safety and integrity of the materials used in the prosthetic discs [35,37]. These findings underscore the importance of selecting appropriate bearing materials and highlight the potential of prosthetic discs, such as CHARITÉ and ProDisc-L, to effectively restore motion while preserving the structural integrity of adjacent bone tissues [38].

5. Conclusions

This study has pioneered an integrated approach that combines 3D biological modeling and finite element interpretation techniques to address lumbar disc degeneration. By employing advanced 3D design and analysis programs tailored to patient-specific needs, our focus has been on minimizing the maximum stresses on artificial discs. This holistic approach aims to extend implantation periods, enhance functional efficiency, and mitigate the risks of disc collapse, thereby preserving the vital anatomical environment. The numerical analysis conducted in this study has provided valuable insights into the impact of various materials and designs on disc stability, considering ROM variations in the addition to the diverse stresses and loads associated with specific clinical cases. While this comprehensive assessment has identified potential weak points, it has also paved the way for the development of reinforcement strategies and adjustments to the proposed model.

However, it is crucial to recognize the limitations of this study. The outcomes are based on computational modeling and simulations, necessitating real-world clinical validation to confirm these results. Moreover, further research is imperative to evaluate the long-term performance and biocompatibility of the proposed models in actual patient scenarios. We advocate for the widespread adoption of this approach in the creation of numerical biomodels and prosthetics, anticipating its potential to revolutionize patient-specific treatments for disc degeneration.

The findings of this study hold promise for improving patient outcomes, emphasizing the advantages of 3D numerical analysis, including high spatial accuracy, time and resource efficiency, and adaptability during the design and manufacturing phases. As the field of medical prosthetics advances, this approach presents exciting prospects for enhancing patient care and optimizing artificial disc replacements. We remain optimistic that future research will refine and expand upon these findings, ultimately leading to improved treatments for individuals suffering from lumbar disc degeneration.

Author Contributions: Conceptualization, methodology, data curation, software: M.A.D. and H.M.N.; investigation, visualization, formal analysis, validation, writing—original draft K.E. and M.S.; supervision, project administration, resources, writing—review and editing: S.S., Y.Z. and D.J. All authors have read and agreed to the published version of the manuscript.

Funding: This research received no external funding.

Institutional Review Board Statement: Not applicable.

Informed Consent Statement: Not applicable.

Data Availability Statement: The datasets generated and/or analyzed during the current study are available from the corresponding author upon reasonable request. The data are not publicly available due to privacy restrictions.

Conflicts of Interest: The authors declare no conflict of interest.

References

1. Ament, J.D.; Yang, Z.; Nunley, P.; Stone, M.B.; Kim, K.D. Cost-Effectiveness of Cervical Total Disc Replacement vs. Fusion for the Treatment of 2-Level Symptomatic Degenerative Disc Disease. *JAMA Surg.* **2014**, *149*, 1231–1239. [CrossRef]
2. Patel, V.V.; Wuthrich, Z.R.; McGilvray, K.C.; Lafleur, M.C.; Lindley, E.M.; Sun, D.; Puttlitz, C.M. Cervical Facet Force Analysis after Disc Replacement versus Fusion. *Clin. Biomech.* **2017**, *44*, 52–58. [CrossRef] [PubMed]
3. DiAngelo, D.J.; Chung, C.; Hoyer, D.; Carson, T.; Foley, K.T. 164. Biomechanical Analysis of the Endplate Fixation Methods of Cervical Total Disc Replacement (TDR) Prostheses to Shear Force Expulsion. *Spine J.* **2021**, *21*, S82–S83. [CrossRef]
4. Kim, D.-W.; Lee, K.-Y.; Jun, Y.; Lee, S.J.; Park, C.K. Friction and Wear Characteristics of UHMWPE against Co-Cr Alloy under the Wide Range of Contact Pressures in Lumbar Total Disc Replacement. *Int. J. Precis. Eng. Manuf.* **2011**, *12*, 1111–1118. [CrossRef]
5. Lazennec, J.Y. Lumbar and Cervical Viscoelastic Disc Replacement: Concepts and Current Experience. *World J. Orthop.* **2020**, *11*, 345–356. [CrossRef] [PubMed]
6. Reeks, J.; Liang, H. Materials and Their Failure Mechanisms in Total Disc Replacement. *Lubricants* **2015**, *3*, 346–364. [CrossRef]
7. Kölle, L.; Ignasiak, D.; Ferguson, S.J.; Helgason, B. Ceramics in Total Disc Replacements: A Scoping Review. *Clin. Biomech.* **2022**, *100*, 105796. [CrossRef] [PubMed]
8. Frost, B.; Camarero-Espinosa, S.; Foster, E. Materials for the Spine: Anatomy, Problems, and Solutions. *Materials* **2019**, *12*, 253. [CrossRef]
9. Pham, M.H.; Mehta, V.A.; Tuchman, A.; Hsieh, P.C. Material Science in Cervical Total Disc Replacement. *Biomed Res. Int.* **2015**, *2015*, 719123. [CrossRef]
10. Biswas, J.K.; Malas, A.; Majumdar, S.; Rana, M. A Comparative Finite Element Analysis of Artificial Intervertebral Disc Replacement and Pedicle Screw Fixation of the Lumbar Spine. *Comput. Methods Biomech. Biomed. Engin.* **2022**, *25*, 1812–1820. [CrossRef]
11. Coric, D.; Parish, J.; Boltes, M.O. M6-C Artificial Disc Placement. *Neurosurg. Focus* **2017**, *42*, V6. [CrossRef]
12. Stephen, D.G.; Prakash; Das, N.K.; Shukla, S. Wear Performance of UHMWPE and PCU Artificial Disc Materials. *J. Inst. Eng. (India) Ser. D* **2022**, *103*, 383–394. [CrossRef]
13. Beatty, S. We Need to Talk about Lumbar Total Disc Replacement. *Int. J. Spine Surg.* **2018**, *12*, 201–240. [CrossRef] [PubMed]
14. Andrieu, K.; Allain, J.; Longis, P.-M.; Steib, J.-P.; Beaurain, J.; Delécrin, J. Comparison between Total Disc Replacement and Hybrid Construct at Two Lumbar Levels with Minimum Follow-up of Two Years. *Orthop. Traumatol. Surg. Res.* **2017**, *103*, 39–43. [CrossRef] [PubMed]
15. Plais, N.; Thevenot, X.; Cogniet, A.; Rigal, J.; Le Huec, J.C. Maverick Total Disc Arthroplasty Performs Well at 10 Years Follow-up: A Prospective Study with HRQL and Balance Analysis. *Eur. Spine J.* **2018**, *27*, 720–727. [CrossRef] [PubMed]
16. Kiyani, S.; Taheri-Behrooz, F.; Asadi, A. Analytical and Finite Element Analysis of Shape Memory Polymer for Use in Lumbar Total Disc Replacement. *J. Mech. Behav. Biomed. Mater.* **2021**, *122*, 104689. [CrossRef] [PubMed]
17. Baliga, S.; Treon, K.; Craig, N.J.A. Low Back Pain: Current Surgical Approaches. *Asian Spine J.* **2015**, *9*, 645–657. [CrossRef]
18. Hollenbeck, J.F.M.; Fattor, J.A.; Patel, V.; Burger, E.; Rullkoetter, P.J.; Cain, C.M.J. Validation of Pre-Operative Templating for Total Disc Replacement Surgery. *Int. J. Spine Surg.* **2019**, *13*, 84–91. [CrossRef]
19. Prokopovich, P.; Perni, S.; Fisher, J.; Hall, R.M. Spatial Variation of Wear on Charité Lumbar Discs. *Acta Biomater.* **2011**, *7*, 3914–3926. [CrossRef]
20. Siskey, R.; Peck, J.; Mehta, H.; Kosydar, A.; Kurtz, S.; Hill, G. Development of a Clinically Relevant Impingement Test Method for a Mobile Bearing Lumbar Total Disc Replacement. *Spine J.* **2016**, *16*, 1133–1142. [CrossRef]
21. Alexander, T.; Antonis, L.; Savvas, S.; Nikolaos, M. Nonintrusive 3D Reconstruction of Human Bone Models to Simulate Their Bio-Mechanical Response. *3D Res.* **2012**, *3*, 5. [CrossRef]
22. Rundell, S.A.; Auerbach, J.D.; Balderston, R.A.; Kurtz, S.M. Total Disc Replacement Positioning Affects Facet Contact Forces and Vertebral Body Strains. *Spine* **2008**, *33*, 2510–2517. [CrossRef] [PubMed]
23. Kong, W.Z.; Goel, V.K. Ability of the Finite Element Models to Predict Response of the Human Spine to Sinusoidal Vertical Vibration. *Spine* **2003**, *28*, 1961–1967. [CrossRef] [PubMed]
24. Choi, J.; Shin, D.-A.; Kim, S. Biomechanical Effects of the Geometry of Ball-and-Socket Artificial Disc on Lumbar Spine: A Finite Element Study: A Finite Element Study. *Spine* **2017**, *42*, E332–E339. [CrossRef] [PubMed]
25. Liao, Z.; Chen, W.; Wang, Z.-H.; Wei, H.-W. Clinical Study of a New Transpedicular Nonfusion Posterior Dynamic Stabilization System for Treating Herniated Lumbar Intervertebral Disks. *Neurosurg. Q.* **2015**, *25*, 427–431. [CrossRef]

26. Auerbach, J.D.; Ballester, C.M.; Hammond, F.; Carine, E.T.; Balderston, R.A.; Elliott, D.M. The Effect of Implant Size and Device Keel on Vertebral Compression Properties in Lumbar Total Disc Replacement. *Spine J.* **2010**, *10*, 333–340. [CrossRef]
27. Hsieh, Y.-Y.; Kuo, Y.-J.; Chen, C.-H.; Wu, L.-C.; Chiang, C.-J.; Lin, C.-L. Biomechanical Assessment of Vertebroplasty Combined with Cement-Augmented Screw Fixation for Lumbar Burst Fractures: A Finite Element Analysis. *Appl. Sci.* **2020**, *10*, 2133. [CrossRef]
28. Goreham-Voss, C.M.; Hyde, P.J.; Hall, R.M.; Fisher, J.; Brown, T.D. Cross-Shear Implementation in Sliding-Distance-Coupled Finite Element Analysis of Wear in Metal-on-Polyethylene Total Joint Arthroplasty: Intervertebral Total Disc Replacement as an Illustrative Application. *J. Biomech.* **2010**, *43*, 1674–1681. [CrossRef]
29. Niosi, C.A.; Zhu, Q.A.; Wilson, D.C.; Keynan, O.; Wilson, D.R.; Oxland, T.R. Biomechanical Characterization of the Three-Dimensional Kinematic Behaviour of the Dynesys Dynamic Stabilization System: An In Vitro Study. *Eur. Spine J.* **2006**, *15*, 913–922. [CrossRef]
30. Noailly, J.; Planell, J.A.; Lacroix, D. On the Collagen Criss-Cross Angles in the Annuli Fibrosi of Lumbar Spine Finite Element Models. *Biomech. Model. Mechanobiol.* **2011**, *10*, 203–219. [CrossRef]
31. Kurtz, S.M.; van Ooij, A.; Ross, R.; de Waal Malefijt, J.; Peloza, J.; Ciccarelli, L.; Villarraga, M.L. Polyethylene Wear and Rim Fracture in Total Disc Arthroplasty. *Spine J.* **2007**, *7*, 12–21. [CrossRef]
32. Schuermans, V.N.E.; Smeets, A.Y.J.M.; van de Kar, L.G.C.; Hermans, S.M.M.; Curfs, I.; Boselie, T.F.M.; van Santbrink, H. A Systematic Review on Neurological Outcomes for Cervical Degenerative Myelopathy after Anterior Decompression Surgery: Motion Preservation vs. Fusion. *Int. J. Spine Surg.* **2022**, *16*, 969–976. [CrossRef]
33. Kurtz, S.M.; MacDonald, D.; Ianuzzi, A.; van Ooij, A.; Isaza, J.; Ross, E.R.; Regan, J. The Natural History of Polyethylene Oxidation in Total Disc Replacement. *Spine* **2009**, *34*, 2369–2377. [CrossRef] [PubMed]
34. Oral, E.; Malhi, A.S.; Wannomae, K.K.; Muratoglu, O.K. Highly Cross-Linked Ultrahigh Molecular Weight Polyethylene with Improved Fatigue Resistance for Total Joint Arthroplasty: Recipient of the 2006 Hap Paul Award. *J. Arthroplasty* **2008**, *23*, 1037–1044. [CrossRef] [PubMed]
35. Hart, N.H.; Nimphius, S.; Rantalainen, T.; Ireland, A.; Siafarikas, A.; Newton, R.U. Mechanical Basis of Bone Strength: Influence of Bone Material, Bone Structure and Muscle Action. *J. Musculoskelet. Neuron. Interact.* **2017**, *17*, 114–139.
36. Karim, L.; Vashishth, D. Role of Trabecular Microarchitecture in the Formation, Accumulation, and Morphology of Microdamage in Human Cancellous Bone: Trabecular Microarchitecture Affects Microdamage. *J. Orthop. Res.* **2011**, *29*, 1739–1744. [CrossRef] [PubMed]
37. Maknickas, A.; Alekna, V.; Ardatov, O.; Chabarova, O.; Zabulionis, D.; Tamulaitienė, M.; Kačianauskas, R. FEM-Based Compression Fracture Risk Assessment in Osteoporotic Lumbar Vertebra L1. *Appl. Sci.* **2019**, *9*, 3013. [CrossRef]
38. Kundu, J.; Pati, F.; Shim, J.-H.; Cho, D.-W. Rapid Prototyping Technology for Bone Regeneration. In *Rapid Prototyping of Biomaterials*; Elsevier: Amsterdam, The Netherlands, 2014; pp. 254–284. ISBN 9780857095992.